THE 4TH INTERNATIONAL CONFERENCE ON ALUMINUM ALLOYS

EFFECT OF MICROSTRUCTURE ON THE FATIGUE CRACK PROPAGATION BEHAVIOR OF HIGH-STRENGTH AL-ZN-MG-CU ALLOYS

F.-J. Grau, A. Gysler, and G. Lütjering
Technical University Hamburg-Harburg, 21071 Hamburg, Germany

Abstract

The constant amplitude fatigue crack growth behavior of 7475 and X-7075 (without Cr) in vacuum and NaCl solution was investigated at R-ratios of 0.1 and 0.7, varying the degree of age-hardening (under- vs. overaged), grain shape anisotropy (pancake vs. near-equiaxed) and concomitant crystallographic texture. It was found for example that an increase in slip planarity (under- as compared to overaged) resulted in increasingly serrated crack front geometries which is thought to be mainly responsible for the observed increase in crack growth resistance, especially at the high R-ratio where no closure was found. Furthermore, a strong textured as compared to a weak textured structure of 7475 exhibited a higher growth resistance at the low R-ratio mainly due to a texture induced higher closure level combined with a rough crack front geometry, while at the high R-ratio (no closure) both structures showed a similar growth resistance as well as comparable crack front geometries.

Introduction

The fatigue crack propagation behavior of long through-cracks in high-strength alloys under constant amplitude loading has been studied extensively in the past. There exists agreement that the resistance against crack growth will be influenced by the fracture properties of the material (e.g. ductility and fracture stress), and at low R-ratios also by crack closure (1,2). Furthermore the additional effect of three-dimensional crack front geometry variations, induced by different microstructures, gained increased attention (1,3-6). It has been found that all microstructural parameters which are able to deviate the local crack front out of the main crack plane are contributing to a higher resistance against fatigue crack propagation. The parameters which are promoting such a beneficial effect are increasing grain sizes (1,5), planar instead of a homogeneous slip distribution (4,5), or a strong texture (3,6).

The purpose of the present study was to contribute to the further understanding of the effect of microstructural variations on the fatigue crack propagation behavior of high-strength Al-alloys by analyzing the concomitant variations in crack front geometry variations as well as considering the fracture properties and at low R-ratios the additional influence of crack closure.

Experimental Procedure

The tests were performed on a commercial 7475 alloy (Kaiser Aluminum Europe) and on a high-purity laboratory alloy X-7075 (Alcan International, U.K.), containing no Cr-dispersoids. The chemical compositions are given in Table I. Alloy X-7075 was tested with an equiaxed grain size of 110 μm in an underaged (UA: 24h 100°C) and an overaged (OA: 48h 180°C) condition. Alloy 7475 was investigated with two different pancake grain structures: condition PCS, having grain dimensions of 1500x250x30 μm in L-, T- and S-directions, respectively, by

Table I. Alloy Compositions (wt.%)

Alloy	Zn	Mg	Cu	Cr	Fe	Si	Mn	Ti
7475	5.80	2.32	1.68	0.23	0.102	0.067	0.022	0.026
X-7075	5.82	2.57	1.51	--	0.04	0.01	0.002	0.011

homogenizing the supplied hot rolled material, and a condition TMT, having reduced grain dimensions of 90x85x30 μm, obtained by a thermomechanical treatment. Both grain structures of 7475 were tested in the underaged condition (UA: 24h 100°C). All mechanical tests were carried out at room temperature, with the loading axis of the specimens being parallel to the rolling direction. Tensile properties were measured on round specimens with gage dimensions of 4 mm diameter and 20 mm length, applying an initial strain rate of $8 \times 10^{-4}\ s^{-1}$. Fatigue crack growth tests (according to ASTM E647) were performed on CT-specimens (8 mm thick, 32 mm wide) under constant amplitude loading at a frequency of 30 Hz using a servocontrolled testing machine. These tests were carried out in vacuum and in 3.5 % NaCl solution (with inhibitor) at R-ratios of 0.1 and 0.7. For a qualitative evaluation of crack closure the compliance of some CT-specimens was measured in the near-threshold regime using conventional back face strain gages. Crack front profiles in the through-thickness direction were analyzed by light micrographs taken from sections perpendicular to the crack growth direction of fractured specimens. In addition some crack front contours were studied by SEM of fracture surfaces of specimens which were fatigue cracked to a defined growth rate and then fractured by continuously increasing the load. Such tests outline the instantaneous crack front contour at a given growth rate which can normally not be seen on the fracture surface of constant amplitude fatigue cracked specimens.

Experimental Results

The tensile properties of all microstructures studied are summarized in Table II.

Table II. Tensile Properties

Alloy/ Condition	Age-Hardening	$\sigma_{0.2}$ (MPa)	UTS (MPa)	σ_F (MPa)	TE (%)	$\varepsilon_F = \ln A_0/A$
X-7075	UA	417	527	775	21	0.47
X-7075	OA	344	433	645	19	0.74
7475/PCS	UA	459	578	702	17	0.20
7475/TMT	UA	434	557	765	21	0.38

The influence of degree of age-hardening on the fatigue crack propagation behavior in vacuum is shown in Fig. 1 for the equiaxed grain structure of X-7075, comparing under- and overaged conditions at R-ratios of 0.1 and 0.7. Crack propagation occurred in a transgranular manner along slip bands in both aging conditions up to growth rates of 10^{-6} m/cycle, independently of R-ratio. The results in Fig. 1 confirm the usually observed higher resistance against crack growth of the planar deforming underaged condition in comparison to the more homogeneously deforming overaged microstructure at low and high R-ratios. However, the underaged condition exhibited pronounced higher growth rates at the high R-ratio of 0.7 as compared to $R = 0.1$, while the overaged condition showed almost no effect by varying the R-ratio.

Examples of through-thickness crack front profiles at a constant propagation rate of 10^{-9} m/cycle are shown in Fig. 2, the crack growth direction being normal to the plane of these light micrographs. The crack front profiles of the underaged condition were found to be very serrated, exhibiting approximately the same roughness at low (Fig. 2a) and at high (Fig. 2b) R-ratios. In

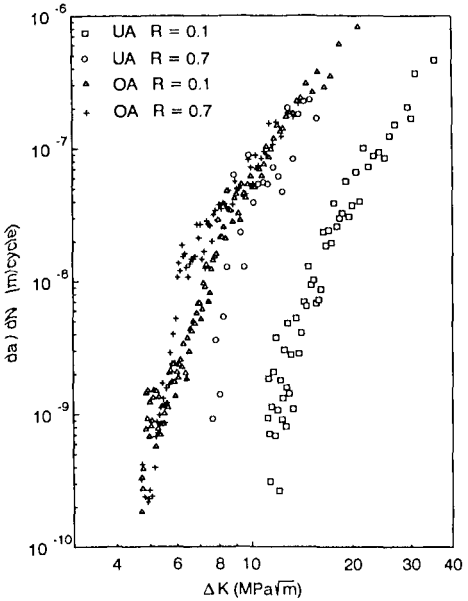

Fig. 1: X-7075, UA vs. OA, Vac.

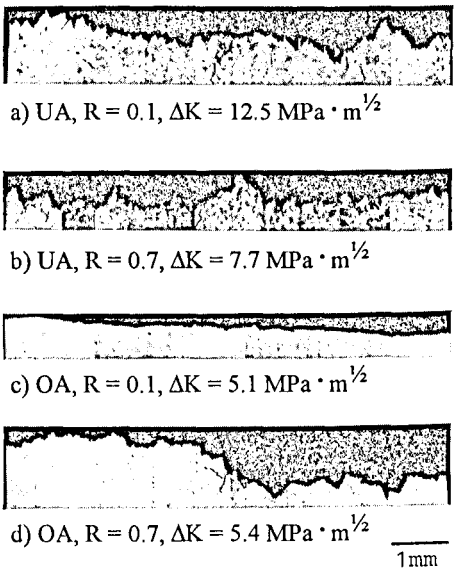

Fig. 2: X-7075, Crack profiles (LM), da/dN = 10^{-9} m/cycle, Vac.

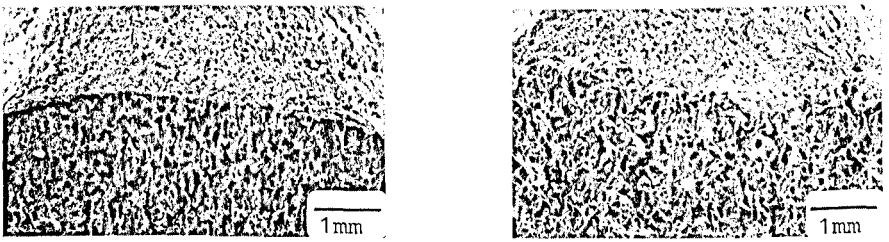

a) R = 0.1 b) R = 0.7

Fig. 3: X-7075, OA, Crack front contours (SEM), da/dN = 10^{-9} m/cycle

Fig. 4: X-7075, OA, R = 0.7, Slip traces (high magnif. of Fig. 2d)

Fig. 5: X-7075, OA, LCF test, R = 0.7 (TEM)

contrast, the overaged microstructure revealed a very flat through-thickness profile at $R = 0.1$ (Fig. 2c) while at a high R-ratio of 0.7 the concomitant profile was found to be much rougher (Fig. 2d), however with more rounded off peaks and valleys as compared to the profiles of the underaged condition (compare Figs. 2b and d).

The crack front contours, marked on the fatigue fracture surfaces by a fracture toughness type test after reaching a growth rate of 10^{-9} m/cycle, are shown in Fig. 3 for the overaged condition at both R-ratios. At $R = 0.1$ the crack front contour was very smooth (Fig. 3a), while at $R = 0.7$ a very irregular contour was observed (Fig. 3b) showing locally advanced crack segments, probably induced by fatigue cracking along the most favorably oriented slip systems in selected grains, leaving unfractured ligaments between those grains. To investigate this rather unusual behavior of the overaged condition at the high R-ratio in more detail, the areas of the crack front profile (Fig. 2d) close to the fracture plane were studied at higher magnifications. These studies revealed strong slip traces in grains adjacent to the tortuous crack plane, as can be seen from the example in Fig. 4, indicating a rather inhomogeneous deformation mode within the plastic zone ahead of the crack tip, despite the heavy overaging treatment of this condition (Table II). Reference investigations at high magnifications of the profiles obtained at $R = 0.1$ (Fig. 2c) did not show such slip traces (7). Additional indications of an inhomogeneous deformation behavior of the overaged condition at high R-ratios were obtained by LCF tests at R-ratios of 0.1 and 0.7. Thin foils from LCF specimens fatigued at $R = 0.7$ exhibited a rather inhomogeneous slip distribution with pronounced slip bands (Fig. 5), while reference studies from LCF specimens at $R = 0.1$ revealed a less inhomogeneous dislocation distribution (7).

Crack closure measurements at propagation rates of 10^{-9} m/cycle showed K_{cl}/K_{max} ratios at $R = 0.1$ of about 0.3 for the underaged and about 0.2 for the overaged condition, while at $R = 0.7$ no indications of closure were observed for both aging conditions.

The as-received commercial 7475 alloy exhibited after a solution heat treatment a pronounced pancake shaped grain structure (termed PCS), which was found to be unrecrystallized having a subgrain size of about 3 μm (7). This structure exhibited a very strong texture, shown in Fig. 6a as {111} pole figure, the marked intensities being "times random". The major component of this texture can best be represented by {123} <412>, while a minor component belongs to {011} <211>. In contrast, the thermomechanical treated 7475 alloy showed a pronounced reduction in grain shape anisotropy (termed TMT) with almost completely recrystallized grains and a very weak texture (Fig. 6b).

The fatigue crack propagation behavior in vacuum of these two underaged microstructures of 7475 is shown in Fig. 7 for R-ratios of 0.1 and 0.7. Crack propagation was found to occur along slip bands in both grain structures. At $R = 0.1$ the highly anisotropic PCS structure showed a higher resistance against crack propagation in comparison to the less anisotropic TMT structure. At $R = 0.7$ this difference in propagation resistance disappeared, the growth curves lying on top of each other (Fig. 7).

Examples of through-thickness crack front profiles at a growth rate of 10^{-9} m/cycle are summarized in Fig. 8 for these two grain structures at low and high R-ratios. All four profiles can be considered as being rough, with a slight tendency for that of the PCS structure at $R = 0.1$ (Fig. 8a) being more serrated than the other three. More detailed studies (7) revealed that the very straight segments of the profile for the PCS structure in most cases crossed more than one grain and (especially at $R = 0.1$) consistently formed "roof"-angles of 50°, which perfectly agreed with crack propagation along the most favorably oriented slip planes of the main texture component (see Fig. 6a). The TMT condition exhibited at both R-ratios highly irregular profiles (Figs. 8c and d) but without such regular angles between adjacent segments of the fracture path as has been found for the PCS structure.

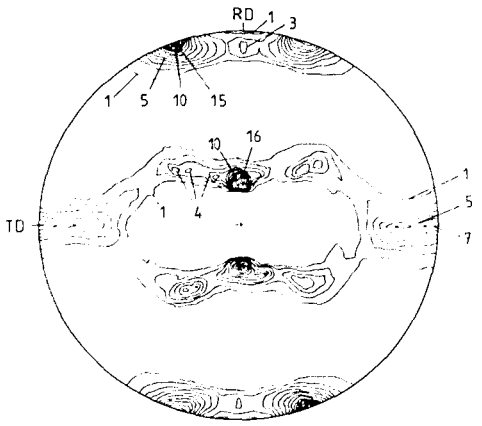

a) PCS

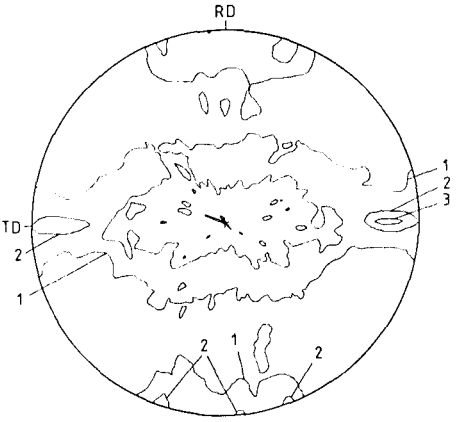

b) TMT

Fig. 6: 7475, UA, {111} Pole figures

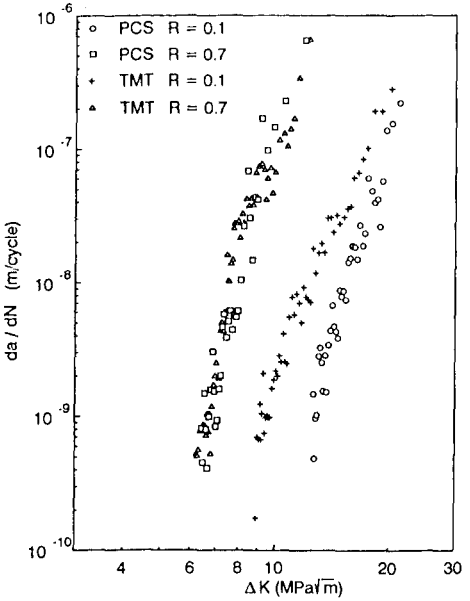

Fig. 7: 7475, UA, PCS vs. TMT, Vac.

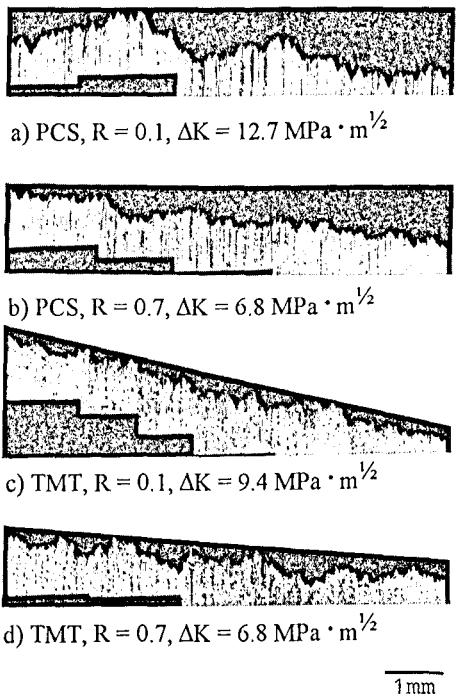

Fig. 8: 7475, UA, Crack profiles (LM), da/dN = 10^{-9} m/cycle, Vac.

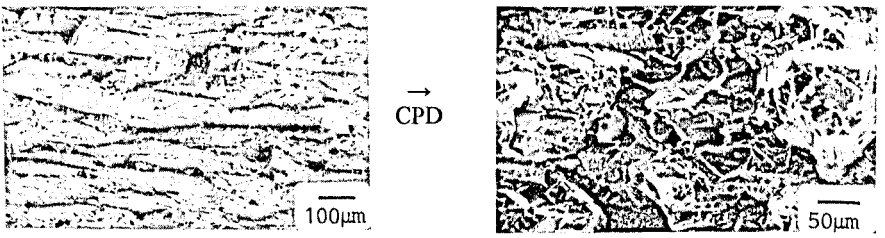

a) PCS, $\Delta K = 12.7$ MPa · $m^{1/2}$ b) TMT, $\Delta K = 9.4$ MPa · $m^{1/2}$

Fig. 9: 7475, UA, Fracture surfaces (SEM), R = 0.1, Vac., da/dN = 10^{-9} m/cycle

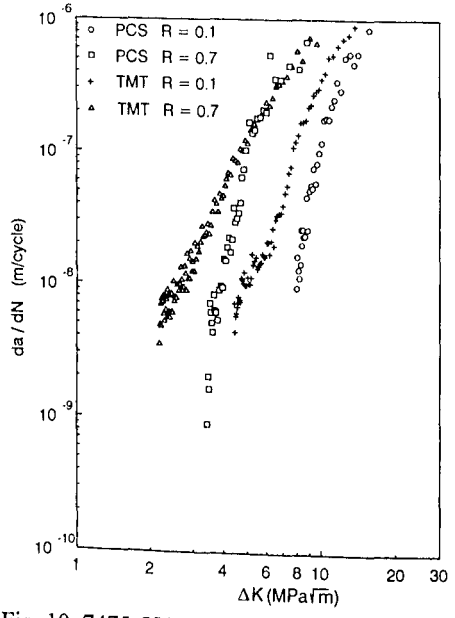

Fig. 10: 7475, UA, PCS vs. TMT, 3.5 % NaCl Sol.

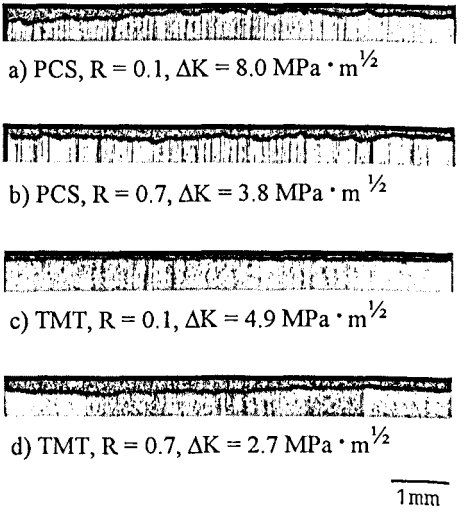

a) PCS, R = 0.1, $\Delta K = 8.0$ MPa · $m^{1/2}$

b) PCS, R = 0.7, $\Delta K = 3.8$ MPa · $m^{1/2}$

c) TMT, R = 0.1, $\Delta K = 4.9$ MPa · $m^{1/2}$

d) TMT, R = 0.7, $\Delta K = 2.7$ MPa · $m^{1/2}$

Fig. 11: 7475, UA, Crack profiles (LM), da/dN = 10^{-8} m/cycle, NaCl Sol.

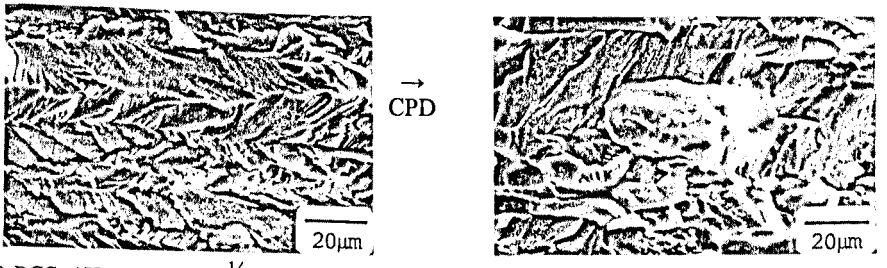

a) PCS, $\Delta K = 8$ MPa · $m^{1/2}$ b) TMT, $\Delta K = 4.9$ m/cycle

Fig. 12: 7475, UA, Fracture surfaces (SEM), NaCl Sol., da/dN = 10^{-8} m/cycle, R = 0.1

Fracture surface studies revealed that crack propagation for the PCS structure occurred mainly in the previously mentioned "roof"-like manner mostly traversing more than one grain along the crack propagation direction (Fig. 9a). At high R-ratio the fracture surface of this PCS structure was less regular, especially the long "roofs" were not observed (7). The recrystallized and more isotropic grain structure (TMT) showed crack propagation along slip bands which varied in crystallographic orientation almost from grain to grain (Fig. 9b).

Crack closure measurements at 10^{-9} m/cycle exhibited K_{cl}/K_{max}-ratios at $R = 0.1$ of about 0.4 for the PCS and about 0.2 for the TMT structures, while again no indications of closure were found at $R = 0.7$ for both grain structures.

The effect of a corrosive 3.5 % NaCl solution on the crack propagation behavior of the two different grain structures (PCS, TMT) of 7475 is shown in Fig. 10, again at R-ratios of 0.1 and 0.7. It can be seen that the anisotropic PCS structure exhibited a higher crack growth resistance (at least below 5×10^{-7} m/cycle) in comparison to the more equiaxed TMT condition, independently of R-ratio. It will be noticed that growth rates in the corrsive environment below about 10^{-8} m/cycle were difficult to measure, esspecially at low R-ratios, because of crack arrest.

The crack front profiles at growth rates of 10^{-8} m/cycle are shown in Fig. 11. Compared to the profiles obtained in vacuum (Fig. 8), those in the corrosive solution can all be considered as very flat, only slight deviations out of the main fracture plane were observed for the PCS structure (Figs. 11a and b). Fracture surface studies revealed a complete transgranular fracture mode for the highly anisotropic PCS structure (Fig. 12a), mainly along {100} cleavage planes as was concluded from the observed squared etch pits on lightly etched fracture surfaces (7), but also some areas with fracture along {111} slip planes. In contrast, the less anisotropic and fine grained TMT structure fractured, besides along {100} cleavage and along {111} slip planes, also along grain boundaries, as shown in Fig. 12b.

Discussion

The results will be discussed on the basis of three important factors known to affect the fatigue crack propagation resistance:

- Fracture properties (e.g. ductility) of the material, keeping in mind that uniaxial tensile properties can only approximate the cyclic properties under plane strain conditions ahead of a propagating fatigue crack.
- Crack front geometry, with the approximation of the three-dimensional crack front by two-dimensional through-thickness crack front profiles or contours.
- Crack closure (at low R-ratios), although there are still problems about quantifying meaningful closure levels.

An effect of crack front geometry variations on crack growth resistance is thought to result from the observation that crack advance occurs locally out of the main fracture plane along the through-thickness direction, preferentially in individual grains, leaving unfractured ligaments between those fractured grains. In order to propagate the overall crack front these ligaments have to be fractured, which obviously reduces the propagation rates. All microstructural or external parameters which are increasing the deviations of the through-thickness crack front from a smooth line are contributing to a higher propagation resistance (1,5).

The observed higher resistance against crack growth of the planar deforming underaged as compared to the more homogeneously deforming overaged condition of X-7075 (Fig. 1) cannot be explained on the basis of fracture properties, which would lead to an opposite ranking (Table II), or with crack closure alone. For example, correcting the crack growth curves in Fig. 1 for the underaged and overaged conditions at $R = 0.1$ with the measured closure values, respectively, would not result in coinciding curves. It is thought therefore that the very tortuous crack front profile of the underaged (Fig. 2a) as compared to the almost flat profile (Fig. 2c) and smooth

contour (Fig. 3a) of the overaged condition seems to be mainly responsible for the observed ranking of these two crack growth curves in Fig. 1. The importance of crack front geometry variations is further illustrated by considering the higher crack growth resistance of the underaged as compared to the overaged condition at the high R-ratio (Fig. 1), where no closure was detected. It is thought that this higher resistance can be explained mainly by the more serrated crack front profile of the underaged (Fig. 2b) as compared to the overaged condition (Fig. 2d). Furthermore, the coinciding propagation curves (certainly by chance) of the overaged condition at low and high R-ratios (Fig. 1) are probably a result of the strikingly different crack profiles, being very flat at $R = 0.1$ (Fig. 2c) but changing to a rough profile at $R = 0.7$ (Fig. 2d), which obviously seems to counterbalance the normally observed higher growth rates at high R-ratios.

Differences in crack closure levels are thought to explain mainly the observed higher crack growth resistance at $R = 0.1$ of the very anisotropic PCS structure of 7475 in comparison to the more equiaxed TMT structure (Fig. 7), together with a contribution of the somewhat rougher profile of the PCS structure (compare Figs. 2a and c). The higher closure of the PCS structure seems to be a consequence of the very strong texture (Fig. 6a), resulting in pronounced shear facets traversing mostly several pancake shaped grains (Figs. 8a and 9c), which is thought to contribute to a pronounced mode II shear displacement at the crack tip. On the other side, the TMT structure with the very weak texture (Fig. 6b) showed a more random orientation of slip band fracture (Fig. 9b) which obviously reduced the amount of mode II shear displacement. At the high R-ratio (no closure) both grain structures exhibited a similar crack growth resistance (Fig. 7), in accordance with the observed almost identical crack front profiles (Figs. 8b and d).

The importance of the fracture properties on the fatigue crack growth resistance, besides other factors (including crack front geometry and closure), was clearly shown by testing the two different grain structures of 7475 in a corrosive NaCl-solution (Fig. 10). The higher resistance of the PCS as compared to the more equiaxed TMT structure, regardless of R-ratio, is thought to result mainly from the observed transgranular fracture mode along {100} planes for the PCS structure (Fig. 12a), as a consequence of the loading axis being parallel to the long boundaries of the pancake grains, in comparison to a pronounced portion of grain boundary fracture together with fracture along {100} planes for the more equiaxed TMT structure (Fig. 12b). The environmentally induced grain boundary fracture is thought to be even more brittle than the transgranular fracture along {100} cleavage planes. In this case the low fracture properties in combination with the very smooth crack profiles (Figs. 11c and d) of the TMT structure result in much lower crack growth resistance as compared to the PCS structure (Fig. 10).

References

1. G. Lütjering, A. Gysler and L. Wagner, Sixth World Conference on Titanium, ed. P. Lacombe, R. Tricot and G. Béranger (Les Ulis, France: Les Editions de Physique, 1988), 71.

2. S. Suresh, A.K. Vasudevan and P.E. Bretz, Met. Trans. 15A, (1984), 369.

3. G.R. Yoder, P.S. Pao, M.A. Imam and L.A. Cooley, Scripta Met. 22, (1988), 1241.

4. K.T. Venkateswara Rao, J.C. McNulty and R.O. Ritchie, Met. Trans. 24A, (1993), 2233.

5. F.-J. Grau, A. Gysler and G. Lütjering, Fatigue 93, ed. J.-P. Bailon and J.I. Dickson (Warley, UK: EMAS, 1993), 623.

6. X.J. Wu, W. Wallace, M.D. Raizenne and A.K. Koul, Met. Trans. 25A, (1994), 575.

7. F.-J. Grau, unpublished results, 1994.